

Blood Vessel Characterization in Colonoscopy Images to Improve Polyp Localization

Joan M. Núñez, Jorge Bernal, Javier Sánchez and Fernando Vilariño

Dept. of Comp. Science, Comp. Vision Center, Edifici O - UAB, 08193 Bellaterra, Spain

Keywords: Colonoscopy, Blood Vessel, Linear Features, Valley Detection.

Abstract: This paper presents an approach to mitigate the contribution of blood vessels to the energy image used at different tasks of automatic colonoscopy image analysis. This goal is achieved by introducing a characterization of endoluminal scene objects which allows us to differentiate between the trace of 2-dimensional visual objects, such as vessels, and shades from 3-dimensional visual objects, such as folds. The proposed characterization is based on the influence that the object shape has in the resulting visual feature, and it leads to the development of a blood vessel attenuation algorithm. A database consisting of manually labelled masks was built in order to test the performance of our method, which shows an encouraging success in blood vessel mitigation while keeping other structures intact. Moreover, by extending our method to the only available polyp localization algorithm tested on a public database, blood vessel mitigation proved to have a positive influence on the overall performance.

1 INTRODUCTION

Colorectal cancer ranks in the third place in incidence and it is the fourth most common cause of cancer death worldwide (Segnan et al., 2011), with about 143.460 new cases expected in 2012 by the most recent estimates of the American Cancer Society for the number of colorectal cancer cases in the United States only (American Cancer Society, 2012) Based on demographic trends, the annual incidence is expected to increase by nearly 80% to 2.2 million cases over the next two decades and most of this increase will occur in the less developed regions of the world. Fortunately, experience in Europe -where colorectal cancer is the second leading cause of cancer deaths with approximately 435.000 new cases diagnosed yearly- has shown that systematic early detection and treatment has the potential to improve control of the disease (Segnan et al., 2011).

Colon cancer's survival rate depends on the stage it is detected on, decreasing from rates higher than 95% in the first stages to rates lower than 35% in stages IV and V (Tresca, A., 2010); hence the importance of detecting it on its early stages by using screening techniques, such as colonoscopy (Hassinger et al., 2010). Colonoscopy is a procedure used to see inside the colon and rectum, which has become the gold standard to also detect and treat inflamed tis-

sue, ulcers, and abnormal growths among others.

During the last decades there is a trend to develop intelligent systems that can provide additional information to medical procedures. Those systems aim to decrease the number of missdetections by providing intelligent support to clinical staff. Some examples include KARDIO (Bratko et al., 1990), (developed to interpret electrocardiograms) or systems that aid on breast cancer detection (Wei et al., 2011) or colonoscopy (Bernal et al., 2011). As depicted on the last reference cited there are several possible domains of application of an intelligent system for colonoscopy, whether it is used as a tool to assist in the diagnosis or as a way to measure objectively the quality of the intervention. Nearly all the existing methods need of an identification of the elements that appear on the endoluminal scene: lumen, wrinkles and folds, blood vessels, polyps, fecal content and specular highlights (see Figure 1).

In this paper we will introduce a method for colonoscopy images which will allow us to separate information referring to blood vessels from scene objects related to the shape of the intestinal wall. By means of our approach we are able to make a difference between 2-dimensional objects, like blood vessels, and 3-dimensional objects, such as folds and polyps. We follow the lines depicted in (Bernal et al., 2012) which pointed out the use of energy images,

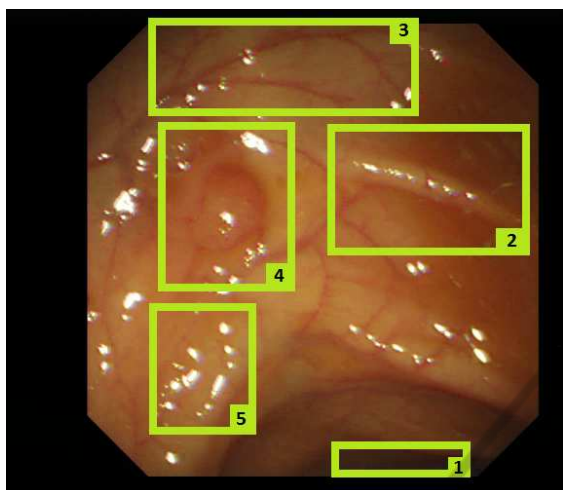


Figure 1: Graphical example of a typical endoluminal scene from a colonoscopy video: 1) Lumen; 2) Wrinkles and folds; 3) Blood vessels; 4) A polyp; 5) Specular highlights.

particularly the output of a valley detector, to make a first approach to endoluminal scene object boundaries detection. We provide a solution to mitigate the effect of blood vessels on an energy image, which shows to be useful to provide a more complete scene description and helps to improve the performance of current polyp localization algorithms.

The structure of the paper is as follows: in Section 2 we present some ideas from other papers that have inspired our work. In Section 3 we present our blood vessels mitigation algorithm. In Section 4 we present our experimental setup and show results of applying our blood vessels mitigation method in colonoscopy images. Finally in Section 5 we show the main conclusions that we extract from our work and present some future research lines.

2 RELATED WORK

As mentioned in Section 1, there are several bibliographic references devoted to the description of elements of the endoluminal scene. Regarding the scope of this paper, we can divide the published works into two different areas, namely: 1) Image enhancement and preprocessing; and 2) Polyp localization.

There are several types of artifacts that are associated to colonoscopy video, which fundamentally consists of color phantoms and specular highlights. Color phantoms are caused by a temporal misalignment of the color channels implied by the use of monochrome CCD cameras in colonoscopy, which means that RGB components are taken at different times and causes a worsening on the quality that must be improved

(Arnold et al., 2011; Dahyot et al., 2008). Specular highlights appear on the intestinal surface as an effect of frontal illumination, causing the apparition of highly saturated regions in the image. There are several approaches to detect and restore the surface below the specular highlights (Arnold et al., 2010; Imai et al., 2011).

Polyp localization concentrates the great majority of the bibliography devoted to intelligent systems for colonoscopy, which could be divided into shape-based polyp localization (Bernal et al., 2012; Zhu and Liang, 2010) and texture-based polyp localization (Ameling et al., 2009; Tjoa and Krishnan, 2003), only to mention a few. One relevant issue, which has not received enough attention, relates to the impact of the different elements of the endoluminal scene -such as folds, wrinkles and vessels- in the overall performance of the polyp localization methods. Particularly, up to our knowledge, there is no existing work that has paid attention to the role of blood vessels in polyp localization, and therefore, there is no concrete bibliography about vessel detection in colonoscopy videos.

However, many different methods have been used to provide a segmentation of blood vessels in two-dimensional images. Most of them have been tested in retinal or angiography images. Despite the wide variability of enhancement steps and segmentation methods they are usually separated in two big groups: pixel-based methods and tracking-based methods (Mendonca and Campilho, 2006).

- Pixel-based methods include different approaches such as kernel-based methods, model-based techniques, classifier-based methods or morphology-based strategies. Kernel-based methods make use of a convolution operator with a particular kernel designed according to a model. The aim of the convolution is usually to extract vessel borders or centerlines. A matched filter approach based on Gaussian kernels is used in some methods to model the cross-section of a blood vessel (Chaudhuri et al., 1989; Hoover et al., 2000). These methods use Gaussian-shaped templates in different orientations and scales to identify vessel profiles. An example of model-based technique (Jiang et al., 2003) proposed a knowledge-guided adaptive thresholding framework where binarization is used to generate object hypotheses. Those hypotheses are only accepted if they pass a verification procedure. Classifier-based methods intend to assign each pixel in the image to the vessel or non-vessel class. In this group we find what the authors called a primitive-based method (Staal et al., 2004). In this method a ridge detection is performed as a first step to achieve a segmenta-

tion of the image. Afterwards, that information is considered to classify regions and pixels. In some examples a bayesian classifier is used after computing feature vectors obtained by Wavelet Gabor responses (Soares et al., 2006) or a neural network is used after computing a feature vector based on moment invariants-based features (Marín et al., 2011). Morphology-based techniques use morphological operators to take advantage of shape characteristics of blood vessels. Morphological operators are usually combined with other techniques. Other authors used the extraction of vessel centerlines combined with local information as the vessel length is followed by an iterative vessel filling phase based on morphological filters (Mendonca and Campilho, 2006). Mathematical morphology can also be combined with curvature evaluation to differentiate vessels from other structures (Zana and Klein, 2001).

- Tracking-based methods aim to obtain the vasculature structure using local information to follow vessel centerlines. Tracking techniques trace vessels from selected starting points which usually correspond to well known anatomical structures. At each point a neighborhood is evaluated to decide whether they are vessel candidate pixels regarding some kind of local information. The process finishes when the pixels evaluated are considered to be end points. Other approaches that can be included in this category are based on deformable or snake models. This techniques place an active contour model near the aimed contour and evolve it iteratively to fit the desired object (Espona et al., 2007).

Many methods using techniques in different categories can also be found. For instance, some approaches combine a classification based on support vector machine followed by a tracking stage based on the Hessian matrix (Xu and Luo, 2010).

In our case the novelty of our approach lies in the consideration of the presence of blood vessels in polyp localization. Our proposal is based on the only available method of automatic polyp localization tested on a public database (Bernal et al., 2012). That work only assesses the influence of specular reflections in the endoluminal scene in polyp localization performance. We intend to improve that approach by considering also the influence of blood vessels.

3 METHODOLOGY

Blood vessels appear in 2-dimensional images as piecewise linear connected components. Unlike other

image types, such as retinal images, the vascular structure in colonoscopy images is not connected in a fully tree-like way nor a single-root tree. The consequence of this is that spatial heuristics such as those mentioned above are not helpful in this case. Therefore, considering the previous definition, intensity valleys in a monochromatic image are a good starting point to detect the vascular structure, as confirmed by the existing related works. However, it becomes an overly broad model in the case of colonoscopy images since the endoluminal scene is made up of several objects of different nature. The problem with this simple blood vessel model is that it also matches other visual components of the endoluminal scene like boundaries of specular highlights, shades, bubble edges, colon wall folds or polyp contours.

In order to separate vessel information from the remaining anatomical structures we propose the following scheming consisting of three different stages, namely: 1) Image preprocessing; 2) Valley detection and 3) Vessel mitigation.

3.1 Pre-processing

Our image preprocessing consists of two different stages: obtaining images from interlaced video and specular highlights detection and inpainting.

Interlaced video frame consists of two sub-fields taken in sequence, each sequentially scanned at odd and even lines of the image sensor (De Haan and Bellers, 1998). In order to digitalize interlaced video the two frames must be combined into a single frame which leads to various undesired visual defects. To avoid that problem we just select the odd frame from each pair of frames and resize it to match the original image proportions.

The method we use for specular highlights detection and inpainting has already been presented (Arnold et al., 2010), which has two different modules: the first one uses color balance adaptative thresholds to determine the parts of specular highlights that present too high intensity to be part of non-specular image content, that is, the saturated pixels on the image. The second module refines the previous specular highlight detection by including pixels nearby to saturated regions of the image that appear to be either shadows of the original artifacts or correspond to the less intense parts of the specular highlights in the image. The specular highlights inpainting is performed on two levels. In the first level the image is modified by replacing all detected specular highlights by the centroid colour of the pixels within a certain distance range of the outline. In the second level a weighted mask is used to combine the modi-

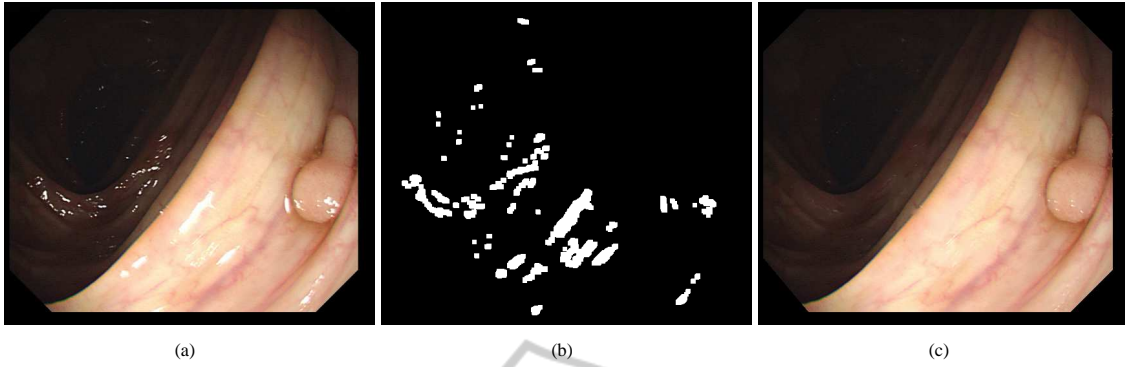


Figure 2: (a) Original image. (b) Specular highlights mask. (c) Output image.

fied image with the original one in a way such pixels inside the specular highlight receive their value from the modified image and pixels far from the highlight have their original value unaltered.

An example of specular highlight detection and inpainting can be seen in Figure 2.

3.2 Valley Detection

Our basic blood vessel model states that blood vessels appear as valleys in monochromatic images. Observation of colonoscopy images in RGB color space shows that the green component is the one that provides greater contrast between vessels and background, which agrees with the generalized idea regarding retinal images (Mendonca and Campilho, 2006). Therefore, the valley detection stage will have as input the preprocessed green component. Since vessels are described as piecewise linear connected components, different linear feature detectors appear as suitable candidates (Papari and Petkov, 2011). Among those detectors, we selected to use matched filters. It does not imply it to be the only possible solution, considering that designing a valley detector is not the aim of this preliminary study.

Blood vessels appear as darker line segments due to its lower reflectance with respect to colon walls. It prompted us to design our filter templates based on second derivatives of anisotropic Gaussian kernels. The kernel values are defined by the oriented Gaussian function described by:

$$G_{(\sigma_x, \sigma_y), \theta} = \frac{1}{(2\pi)\sigma_x\sigma_y} e^{-\left(\frac{\tilde{x}^2}{2\sigma_x^2} + \frac{\tilde{y}^2}{2\sigma_y^2}\right)} \quad (1)$$

where (σ_x, σ_y) are the scales in the corresponding axis and θ is the rotation angle of the filter. \tilde{x} and \tilde{y} are the coordinates given by the rotation angle. Hence they are defined as:

$$\begin{aligned} \tilde{x} &= x \cos \theta + y \sin \theta \\ \tilde{y} &= x \sin \theta - y \cos \theta \end{aligned} \quad (2)$$

As we use anisotropic Gaussians with $\sigma = \sigma_x = 2\sigma_y$, the Gaussian function results in:

$$G_{\sigma, \theta} = \frac{1}{(2\pi)2\sigma^2} e^{-\left(\frac{\tilde{x}^2}{2(2\sigma)^2} + \frac{\tilde{y}^2}{2\sigma^2}\right)} \quad (3)$$

Therefore, since we are modelling blood vessel profiles with second derivatives of anisotropic Gaussian kernels, the kernel will be defined as:

$$\partial_{\tilde{y}}^2 G_{\sigma, \theta} = \frac{\tilde{y}^2 - 1}{\sigma^4} G_{\sigma, \theta} \quad (4)$$

We apply a normalization so that the geometry of the valleys is prioritized:

$$G_{\sigma, \theta}^N := \frac{\|\partial_{\tilde{y}}^2 G_{\sigma, \theta} * I\|}{\|\partial_{\tilde{y}}^2 G_{\sigma, \theta}\| \|I\|} \quad (5)$$

where $\|\cdot\|$ stands for the L^2 integral norm and $*$ denoting the convolution operator.

The kernels are applied for 8 equally distributed orientations and scales $\sigma = [2, 4, 6]$, which cover all vessels width in our test dataset. It all means we have 24 output images, each of them corresponding to a determined orientation and scale. Hence, the output $I_{valleys}$ must be a combination of all of them, defined as follows:

$$I_{valleys} = \max_{i,j} \left(G_{\sigma^i, \theta^j}^N \right) \quad (6)$$

Prior to the valley detection method described above, structure preserving diffusion (Gil et al., 2009) is applied in order to remove image surface irregularities while preserving image structure. The output of this stage, $I_{valleys}$, is a gray level image in which the higher the value of a pixel, the higher the chances of that pixel to be part of a valley. See Figures 3(a), 3(b) and 3(c) for an example of the process described so far.

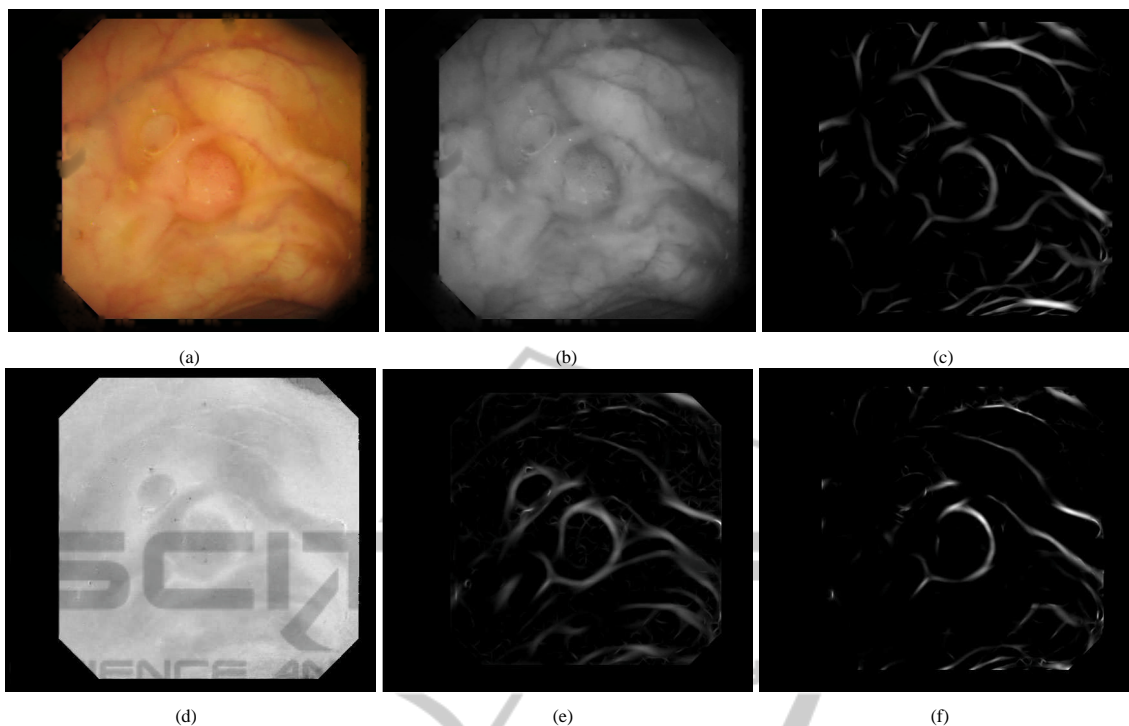


Figure 3: (a) Image after highlight removal. (b) Green component. (c) Valley energy image. (d) Saturation (HSV space). (e) Shadings energy image. (f) Final output energy image.

3.3 Vessel Mitigation

With regard to intensity values, both blood vessels and shadings from folds and wrinkles appear as elongated regions which are darker than intestinal walls in the background. Previous work showed that shadings from all the endoluminal structures can be approximated by the Phong's model (Bernal et al., 2012), which includes ambient, diffused and specular components. Specular reflections have a spectral distribution nearly the same as the incident light but the diffuse component depends also on the object properties (Shafer, 1985). The ambient component is a non-directional source that groups environmental inter-reflections (Blinn, 1977). The resulting color of a given region in the endoluminal scene will depend on the orientation of the light source, which is coupled to the camera with its same orientation. In that sense, the dark areas created by folds are never oriented to the light source, and thus the nature of their color is conditioned by this orientation. Local variations of surface orientation in folds affect to the components in a different way. Specular reflection contribution decreases more quickly than the diffuse component in regions not oriented to the camera. Besides, since the diffuse component depends on the surface reflective properties and the surface orientations, regions

which are not oriented to the camera, such as parts of folds and wrinkles, will appear as more saturated in color. In these regions the contribution of the specular component is lower, and the diffuse component will contribute to a higher saturation in color. Conversely, blood vessels are flat visual features that can be found in regions with any kind of orientation so that the nature of their color is not affected differently than the surrounding areas.

These considerations about the nature of the objects in the endoluminal scene based on its illumination led us to explore HSV color space (Joblove and Greenberg, 1978), since it decouples the intensity of the image -which conveys no discriminative power between vessels and shadings- from its chromatic components. In HSV space H, S and V stand for hue, saturation and value, respectively. Hue is associated with the dominant wavelength in the color spectrum. Saturation refers to the amount of white light mixed with that dominant wavelength and it is defined as:

$$S = \frac{\max(r, g, b) - \min(r, g, b)}{\max(r, g, b)} = 1 - \frac{\min(r, g, b)}{\max(r, g, b)} \quad (7)$$

Assuming that colon wall properties remain unchanged at folds and wrinkles, the different color they

show is to be related exclusively to changes in the illuminant contribution. Therefore, fold/wrinkle regions will have higher levels of saturation than the neighbouring colon wall regions. An exhaustive test on our test dataset confirmed that color-saturation levels in vessel regions appear to be systematically closer to the levels of the adjoining background intestinal walls (see an example in Figure 3(d)). Consequently, fold/wrinkle regions can be described as piecewise linear connected regions in the saturation component image. An energy image describing the presence of folds and wrinkles in the scene, $I_{shadings}$, can be computed using the techniques exposed in Section 3.2 taking the complementary of saturation as input. Figure 3(e) shows an example of this result. The final output image, I_{out} , (see Figure 3(f)) will be computed as:

$$I_{out}(x, y) = I_{valleys}(x, y)I_{shadings}(x, y) \quad (8)$$

This resulting image is expected to enhance shadings from folds, wrinkles and polyps while mitigating blood vessels.

4 EXPERIMENTAL RESULTS

4.1 Experimental Setup

One of the problems when testing the performance of an algorithm is that validation should be done on a consistent database. Sadly it is very difficult to find any online database with data from colonoscopy video, as they are usually confidential. Nevertheless, a public dataset from colonoscopy video has been made available recently (Machine Vision Group, CVC, 2012). This dataset consists of 380 images from 15 different colonoscopy videos. Each frame contains a polyp but the authors have focus on showing as many different polyp appearances as possible. From now on, we will referred to this dataset as the CVC-ColonDB.

As we are interested on blood vessels mitigation we selected and annotated a subdataset of 29 images following as a criterion the presence of blood vessels. Blood vessels have been labelled manually by experts in order to create blood vessels masks. This dataset will be referred as the Vessel Dataset. An example of our Vessel Dataset can be seen in Figure 4.

Several experiments were developed to assess quantitatively the performance of our method on mitigating blood vessels. More specifically, we want to compare the energy corresponding to blood vessels in both the valley energy image and the valley energy image after blood vessel mitigation.

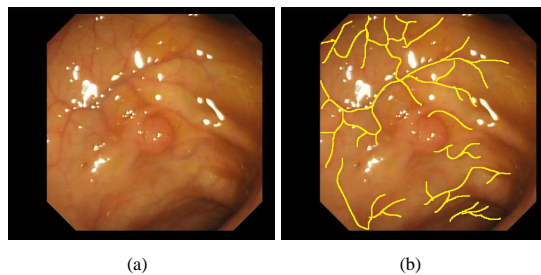


Figure 4: Example of Vessel Dataset: (a) Original image. (b) Blood vessels mask superimposed on the original image.

As our vessel masks have been created only as descriptors of its trace without any width information, we dilated the masks of blood vessels using morphological operators to provide us with a region of blood vessel influence. It allows us to separate the energy in blood vessel regions from the energy in non-vessel regions. Given L_v as the vessel mask and \oplus as the dilation operator, vessel energy, E_v , in the considered energy image I is defined in 9.

$$E_v = \frac{\sum_{(x,y) \in I} I(x,y)(L_v \oplus S_r)(x,y)}{\sum_{(x,y) \in I} I(x,y)} * 100 \quad (9)$$

Consequently, the total energy in an image, E_{total} , will satisfy:

$$E_{total} = E_v + E_{nv} = 100; \quad (10)$$

which describes the balancing of energy between vessels and non-vessels as a percentage of contribution.

4.2 Vessel Mitigation

The proposed metrics have been computed for both the valley energy images and the valley energy images after vessel energy removal. Figure 5(a) shows E_v performance metric for each image in the whole Vessel Dataset already introduced. The figure allows us to verify the decrease of energy in areas previously identified as blood vessels as well as the variability of that decrease. The decrease of energy referred to vessels depends on the content of visual objects on the image. Images which had a high degree of vascular content prior to our processing and no folds interfering with them suffer an important decrease. Nevertheless, images whose vascular content was low or its trace is close or strongly crossed by folds do not show remarkable differences in terms of vessel energy, as expected. An example of both situations can be seen in Figure 6. First row in the figure shows an example where the input image has a large amount of vascular

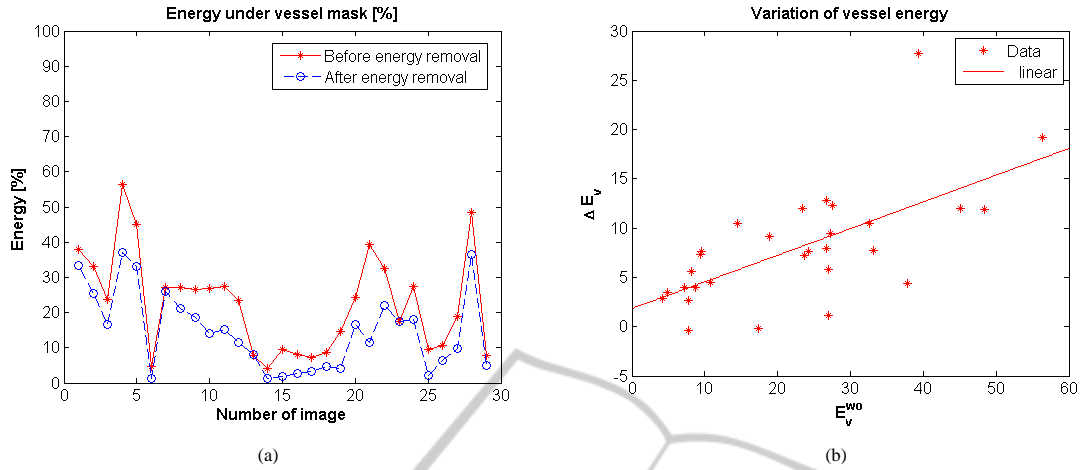


Figure 5: (a) Energy under vessel mask for each image. (b) Variation of vessel energy regarding vessel energy at input.

content in a clear surface not interfered with shades or folds. The example in the second row contains few vascular content and many clear folds. For this reason, folds and shades keep most of the image energy after vessel detection and vessel energy removal has less impact. Figure 5(b) plots the variation of energy under vessel masks regarding the energy under vessel mask prior to our removal step. The increase of energy, ΔE_v , is defined so that a positive value corresponds to vessel energy decrease:

$$\Delta E_v = E_v^{wo} - E_v^w \quad (11)$$

where E_v^{wo} is the energy image without vessel mitigation and E_v^w is the energy image with vessel mitigation. We can see that the energy decrease is related to the energy at the beginning of the process (Pearson correlation coefficient of 0.65). The results regarding energy in non-vessel regions are the complementary of the ones presented in Figure 5(a) as stated in Equation 10. Therefore, we can also affirm that regions which has been manually identified as non-vessels does not suffer substantial energy decrease.

4.3 Application to Polyp Localization

As mentioned in Section 1, our objective is to provide a first approximation of a blood vessels characterization. This characterization could be useful to provide a better scene description, but it also shows to provide relevant information for some other applications such as helping in polyp localization. There are several approaches to polyp localization and some of them have been introduced in Section 2. In this section we will measure how the characterization of blood vessels could be useful to improve the only current available results on polyp localization that are

obtained in a public database, already introduced as CVC-ColonDB database (Bernal et al., 2012). In our case, we will use the output of our processing scheme as the depth of valleys image, and we will measure the accumulation of energy by using the SA-DOVA descriptor. SA-DOVA descriptor defines an accumulation image by using data from the depth of valleys image. The value for each pixel is calculated in the following way: a series of sectors centered on each pixel accumulate, for each direction, the maxima of the depth of valleys image. Therefore, the accumulation value is computed as:

$$Acc(x) = \int_{\alpha=0}^{\alpha=2\pi} \max_{r \in [R_{min}, R_{max}]} E_{radii}(\alpha) d\alpha \quad (12)$$

where E_{radii} is equal to:

$$E_{radii}(\alpha) = E(x + r * (\cos(\alpha), \sin(\alpha))) \quad (13)$$

where R_{min} and R_{max} are the minimum and maximum radii of the sectors used to generate the accumulation image and E the energy image. Our hypothesis is that by identifying which parts of the energy image correspond to blood vessels information we could be able to mitigate their effect and check if the energy inside and outside the polyp changes. The metric that we will use in this experiments is:

$$E_p = \frac{\sum_{(x,y) \in I} I(x,y) L_p(x,y)}{\sum_{(x,y) \in I} I(x,y)} * 100 \quad (14)$$

where L_p is the polyp mask from the Polyp Dataset. We measure the percentage of energy inside the polyp

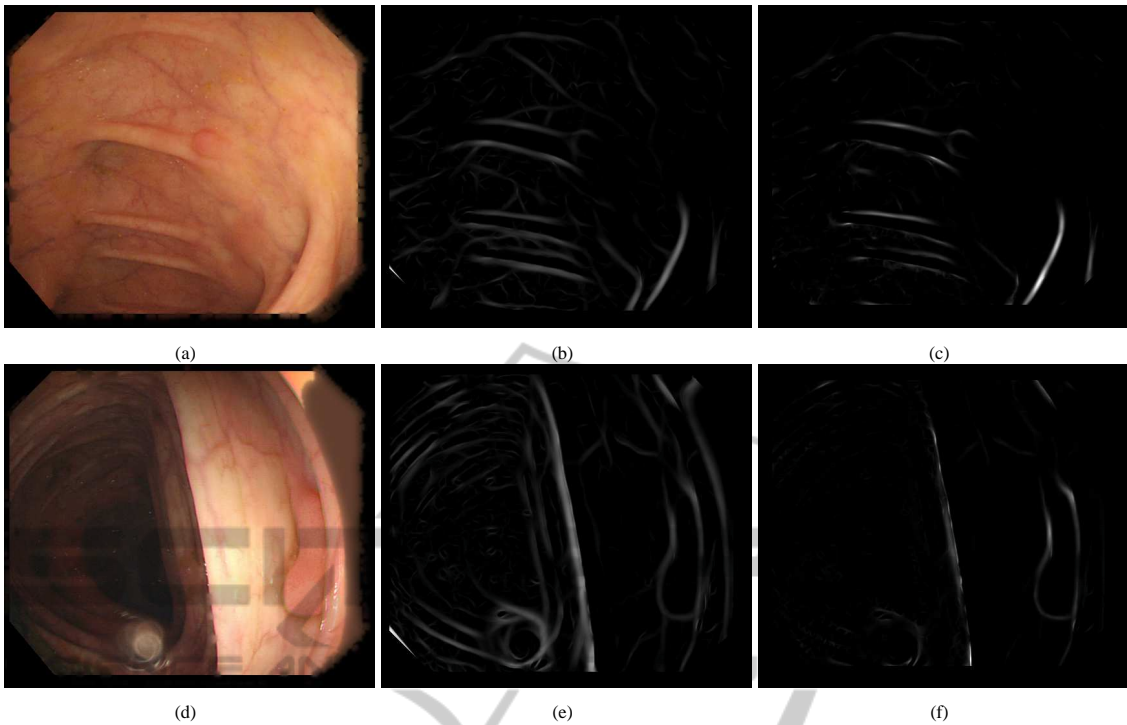


Figure 6: Example 1: (a) Input image. (b) Valley energy image. (c) Energy image after energy removal). Example 2: (d) Input image. (e) Valley energy image. (f) Energy image after energy removal.

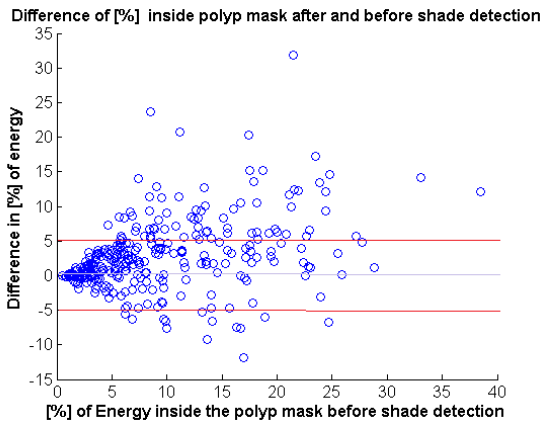


Figure 7: Difference of percentage of energy under polyp mask before and after blood vessel energy mitigation.

mask whereas the energy outside the polyp will be the complementary. We expect that a polyp localization decision scheme based on the amount of energy concentrated on some area of the image will benefit from a blood vessel mitigation system which reduces the presence of vessel energy. We measure the increment of energy inside the polyp mask as:

$$\Delta E_p = E_p^w - E_p^{wo} \tag{15}$$

where E_p^{wo} stands for the energy image without vessel

mitigation and E_p^w stands for the energy image with vessel mitigation. That difference of energy, ΔE_p , referred to E_p^{wo} is plotted in Figure 7. Table 1 shows that we improve the amount of energy inside the polyp mask in a large majority of images (217). This is true even considering that an increase or decrease lower than a 5% can be assumed as not significant (74 improved images).

Table 1: Difference of percentage of energy under polyp mask with and without blood vessel mitigation.

ΔE_p	# of images
> 0	217
$> 5\%$	74
$< -5\%$	13

To conclude with this section, we will show the direct impact that blood vessels mitigation has on polyp localization. In this case we will use the same polyp localization criteria than the one depicted in (Bernal et al., 2012), that is, measuring if the maxima of the accumulation image is placed inside the polyp mask. We can see a comparison between the results before and after applying our blood vessel energy mitigation in Table 2.

As we can see from Table 2, by applying our blood vessel mitigation algorithm the maxima of the accumulation image is placed inside the polyp mask in 47

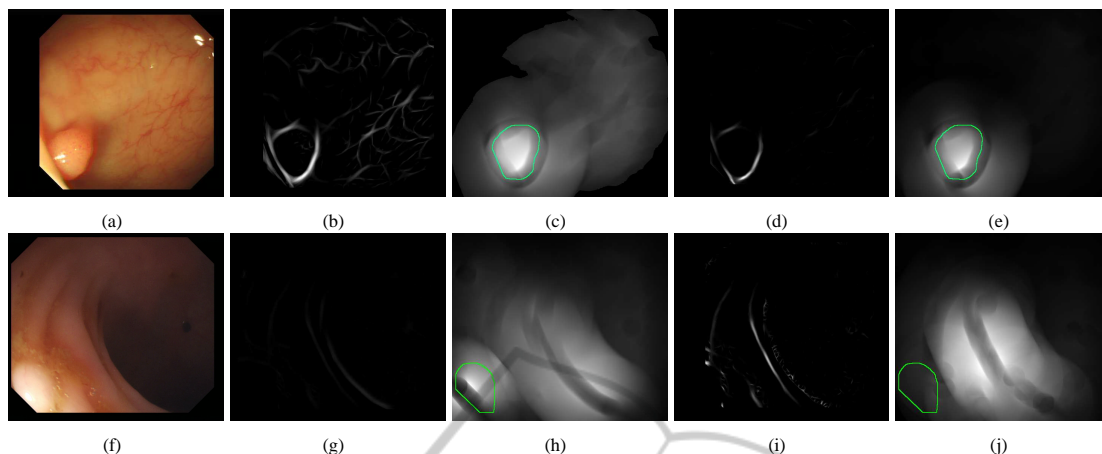


Figure 8: Example 1: (a) Original images. (b) Energy image before shade detection. (c) Accumulation image before shade detection. (d) Energy image after shade detection. (e) Accumulation image after shade detection (polyp region marked in green). Example 2: (f) Original images. (g) Energy image before shade detection. (h) Accumulation image before shade detection. (i) Energy image after shade detection. (j) Accumulation image after shade detection (polyp region marked in green).

Table 2: Polyp localization results (placing accumulation maxima inside polyp mask): comparing results using vessel mitigation with no vessel mitigation.

	# of images	Polyp Dataset %
improved	47	15.67%
worse	8	2.67%
same	245	81.67%

more images (15.67%), the results were worse for 8 (2.67%), and no modification took place for 245 images (81.67%). This preliminary study shows that blood vessel mitigation can be a key part in the improvement of a polyp localization scheme, as it does have an impact on direct polyp localization results. Finally we show in Figure 8 some qualitative results of the comparison of the accumulation images before and after applying our processing scheme. The first row shows a positive example, where the percentage of energy inside the polyp grows after applying vessel mitigation whereas the second row shows a negative example.

5 CONCLUSIONS

In this paper we introduced a characterization for blood vessels which allowed us to model them differently than other objects in an endoluminal scene, more specifically folds and wrinkles. We presented a procedure for mitigating blood vessels which consists of three stages: 1) Image preprocessing, to correct artifacts from the original image such as specular highlights; 2) Valley detection, to provide a first charac-

terization of the objects in the image, and 3) Valley mitigation as a novel method which aims to discriminate between objects that have shades from objects that do not have them, such as blood vessels.

Our experiments show an encouraging trend, indicating that there is a decrease of energy on blood vessel areas. Quantitative results suggest that our method is able to achieve vessel mitigation successfully and that mitigation is more important on images with more blood vessel content. Our procedure was used to improve the only existing polyp localization method that has been tested in a public database. As expected, the polyp localization decision scheme -based on the amount of energy concentrated on some area- benefited from a blood vessel mitigation system which reduces the presence of vessel energy. This is the first time that the impact of blood vessels in polyp localization has been measured quantitatively, proving that their presence makes it harder to identify 3-dimensional objects such as polyps.

Regarding future work, vessel characterization should be validated on a bigger manually labelled dataset. It should also involve the consideration of the superposition of blood vessels and other elements in the endoluminal scene. The appearance of vessels in folds must prompt us to add more information to the improved characterization presented in this work.

ACKNOWLEDGEMENTS

This work was supported in part by the Spanish Gov. grants TIN2012-33116, MICINN TIN2009-

10435 and Consolider 2010 MIPRCV (CSD2007-00018), and the UAB grants 471-01-2/2010 and 471-01-3/2008.

REFERENCES

- Ameling, S. et al. (2009). Texture-based polyp detection in colonoscopy. *Bildverarbeitung für die Medizin 2009*, pages 346–350.
- American Cancer Society (2012). What are the key statistics about colorectal cancer? [Online; accessed 7-September-2012].
- Arnold, M. et al. (2010). Automatic segmentation and inpainting of specular highlights for endoscopic imaging. *Journal on Image and Video Processing*, 2010:9.
- Arnold, M. et al. (2011). Quality Improvement of Endoscopy Videos. In *Proceedings of the 8th IASTED International Conference on Biomedical Engineering*, Innsbruck, Austria.
- Bernal, J. et al. (2011). *Colonoscopy Book 1: Towards Intelligent Systems for Colonoscopy*. In-Tech.
- Bernal, J. et al. (2012). Towards automatic polyp detection with a polyp appearance model. *Pattern Recognition*, 45(9):3166 – 3182.
- Blinn, J. (1977). Models of light reflection for computer synthesized pictures. In *ACM SIGGRAPH Computer Graphics*, volume 11, pages 192–198. ACM.
- Bratko, I. et al. (1990). KARDIO: a study in deep and qualitative knowledge for expert systems. *MIT Press*.
- Chaudhuri, S. et al. (1989). Detection of blood vessels in retinal images using two-dimensional matched filters. *IEEE Transactions on medical imaging*, 8(3):263–269.
- Dahyot, R., Vilariño, F., and Lacey, G. (2008). Improving the quality of color colonoscopy videos. *Journal on Image and Video Processing*, 2008:1–7.
- De Haan, G. and Bellers, E. (1998). Deinterlacing-an overview. *Proceedings of the IEEE*, 86(9):1839–1857.
- Espona, L. et al. (2007). A snake for retinal vessel segmentation. *Pattern Recognition and Image Analysis*, pages 178–185.
- Gil, D. et al. (2009). Structure-preserving smoothing of biomedical images. In *Computer Analysis of Images and Patterns*, pages 427–434. Springer.
- Hassinger, J. et al. (2010). Effectiveness of a Multimedia-Based Educational Intervention for Improving Colon Cancer Literacy in Screening Colonoscopy Patients. *Diseases of the Colon & Rectum*, 53(9):1301.
- Hoover, A. et al. (2000). Locating blood vessels in retinal images by piecewise threshold probing of a matched filter response. *Medical Imaging, IEEE Transactions on*, 19(3):203–210.
- Imai, Y. et al. (2011). Estimation of multiple illuminants based on specular highlight detection. *Computational Color Imaging*, pages 85–98.
- Jiang, X. et al. (2003). Adaptive local thresholding by verification-based multithreshold probing with application to vessel detection in retinal images. *Pattern Analysis and Machine Intelligence, IEEE Transactions on*, 25(1):131–137.
- Joblove, G. and Greenberg, D. (1978). Color spaces for computer graphics. *ACM SIGGRAPH Computer Graphics*, 12(3):20–25.
- Machine Vision Group, CVC (2012). Cvc-colondb: A database for assessment of polyp detection. [Online; accessed 24-July-2012].
- Marín, D. et al. (2011). A new supervised method for blood vessel segmentation in retinal images by using gray-level and moment invariants-based features. *Medical Imaging, IEEE Transactions on*, 30(1):146–158.
- Mendonca, A. and Campilho, A. (2006). Segmentation of retinal blood vessels by combining the detection of centerlines and morphological reconstruction. *Medical Imaging, IEEE Transactions on*, 25(9):1200–1213.
- Papari, G. and Petkov, N. (2011). Edge and line oriented contour detection: State of the art. *Image and Vision Computing*, 29(2-3):79–103.
- Segnan, N. et al. (2011). *European guidelines for quality assurance in colorectal cancer screening and diagnosis*. Luxembourg: Publications Office of the European Union.
- Shafer, S. (1985). Using color to separate reflection components. *Color Research & Application*, 10(4):210–218.
- Soares, J. et al. (2006). Retinal vessel segmentation using the 2-d gabor wavelet and supervised classification. *Medical Imaging, IEEE Transactions on*, 25(9):1214–1222.
- Staal, J. et al. (2004). Ridge-based vessel segmentation in color images of the retina. *Medical Imaging, IEEE Transactions on*, 23(4):501–509.
- Tjoa, M. and Krishnan, S. (2003). Feature extraction for the analysis of colon status from the endoscopic images. *BioMedical Engineering OnLine*, 2(9):1–17.
- Tresca, A. (2010). The Stages of Colon and Rectal Cancer. *New York Times (About.com)*, page 1.
- Wei, J. et al. (2011). Computer-aided detection of breast masses: Four-view strategy for screening mammography. *Medical Physics*, 38:1867.
- Xu, L. and Luo, S. (2010). A novel method for blood vessel detection from retinal images. *BioMedical Engineering OnLine*, 9(1):14.
- Zana, F. and Klein, J. (2001). Segmentation of vessel-like patterns using mathematical morphology and curvature evaluation. *Image Processing, IEEE Transactions on*, 10(7):1010–1019.
- Zhu, H. and Liang, Z. (2010). Improved Curvature Estimation for Shape Analysis in Computer-Aided Detection of Colonic Polyps. *Beijing, China*, page 19.